JOURNAL OF CHEMICAL INFORMATION AND MODELING

Article

pubs.acs.org/jcim

QM/MM Simulations of Amyloid-β 42 Degradation by IDE in the Presence and Absence of ATP

Carlos H. B. da Cruz and G. M. Seabra*

Departamento de Química Fundamental, Universidade Federal de Pernambuco, Av. Jornalista Aníbal Fernandes, s/n, Cidade Universitária, Recife-PE, Brazil, 50.740-560

ABSTRACT: The ability of the insulin-degrading enzyme (IDE) to degrade amyloid-β 42 (Aβ42), a process regulated by ATP, has been studied as an alternative path in the development of drugs against Alzheimer's disease. In this study, we calculated the potential of mean force for the degradation of Aβ42 by IDE in the presence and absence of ATP by umbrella sampling with hybrid quantum mechanics and molecular mechanics (QM/MM) calculations, using the SCC-DFTB QM Hamiltonian and Amber ff99SB force field. Results indicate that the reaction occurs in two steps: The first step is characterized by the formation of the intermediate. The second step is characterized by breaking the peptide bond of the substrate, the latter being the rate-determining step. In our simulations, the activation energy barrier in the absence of ATP is 15 ± 2 kcal mol^{-1}, which is 7 kcal mol^{-1} lower than in the presence of ATP, indicating that the presence of the nucleotide decreases the reaction rate by about 10^5 times.

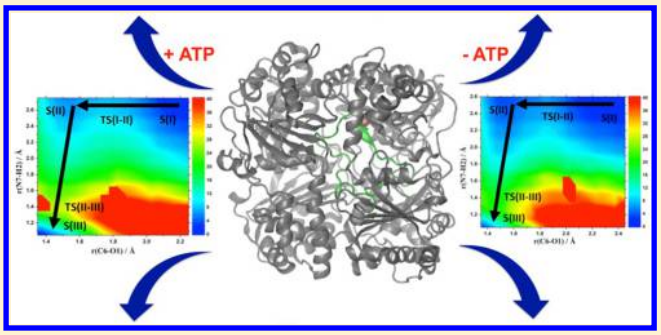

INTRODUCTION

Although more than a century has passed since the discovery of Alzheimer's disease (AD), little is known about the sequence of events that cause it. However, the close relationship between excess of the peptide amyloid-β 42 (Aβ42) and events leading to neurodegeneration has been widely investigated.[1−4] These findings have created a framework for the main lines of research.[5−7] Currently, it is believed that the cure is strongly related to the regulation of brain amyloid levels, either by inhibiting the enzymes involved in the production[8] or activating the ones involved in the degradation processes of the polypeptide.[9−11] Over the past few years, emphasis has been placed on the determination of proteolytic pathways by which amyloid is regulated.[12−16] In this sense, the neprilysin (NEP) and insulin-degrading enzyme (IDE) are those that best satisfy this role.[12]

Present in various tissues including cerebrovascular endothelial cells,[17,18] IDE (also called insulinase) is a promiscuous zinc metalloproteinase from the M16A family found in bacteria, fungi, plants, and animals.[19] It was historically linked to breakage of insulin and later the degradation of other active biomolecules, including Aβ42.[20,21] Its tertiary structure is composed of four domains (domains 1−4) in the form of $\alpha\beta$-sandwich (Figure 1). The N-terminal half (IDE-N, domains 1 and 2) is connected to the C-terminal half (IDE-C, domains 3 and 4) by a flexible loop of 28 residues. The loop articulates movements between the two halves, allowing the existence of open and closed conformations. When closed, IDE forms a catalytic chamber of triangular base with dimensions 35 Å × 34 Å × 30 Å and 1300 Å^3 volume. The active site is located in domain-1 inside the catalytic chamber and consists of a Zn^{2+} ion, three amino acids (HIS108, HIS112, and GLU189), and a water molecule, all coordinated to the zinc (Figure 1). The enzyme also has a distal site located in domain-2, 30 Å away from the active site, whose function is to facilitate the binding of the substrate and activate the neighboring subunit via allosteric effects.[22,23]

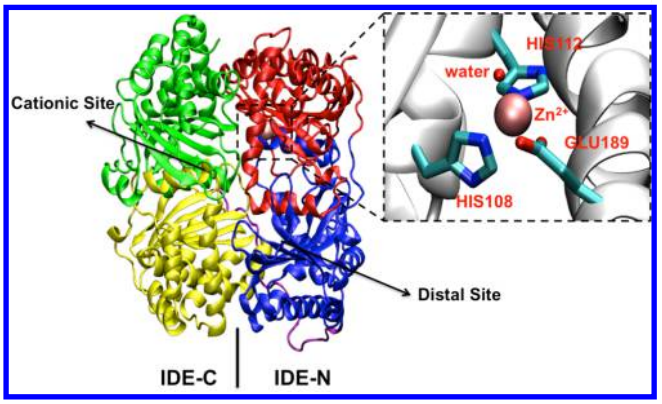

Figure 1. Experimental structure of IDE (PDB code: 2GJ4). Domains 1, 2, 3, and 4 are colored red, blue, yellow, and green. IDE-N and C and the cationic and distal site are indicated. The structure of active site is shown on the right.

Adenosine triphosphate (ATP) is an endogenous regulator of IDE. IDE is an activator in the breaking of short substrates, and it also works as an inhibitor in breaking long substrates,

Received: September 8, 2014
Published: December 24, 2014

DOI: 10.1021/ci500544c
J. Chem. Inf. Model. 2015, 55, 72−83

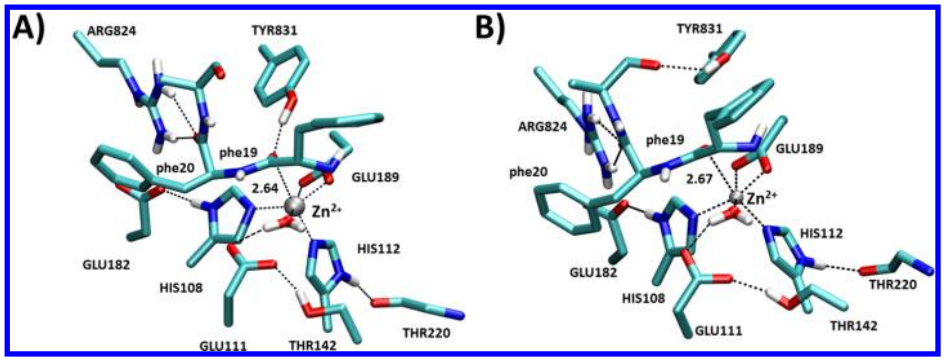

Figure 2. Initial geometry around the active site: (A) system without ATP and (B) system with ATP.

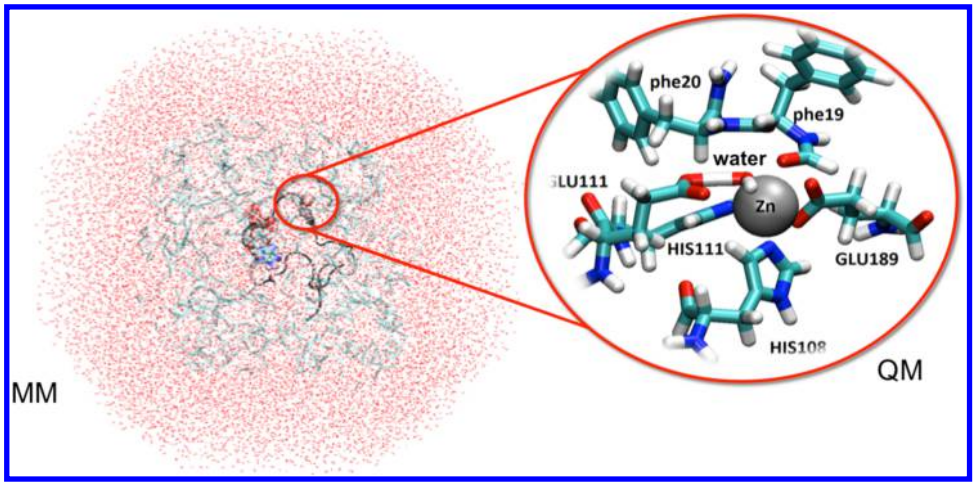

Figure 3. MM and QM Region.

such as Aβ42.[11,24,25] The presence of the nucleotide also induces a quaternary structure change in IDE, from dimers to monomers, eliminating the communication between the subunits and thereby inhibiting the allosteric activation mechanism.[24] It has been suggested that when bound to the cationic site in IDE-C ATP breaks the electrostatic equilibrium that holds the terminal halves in the closed conformation (inactive form), hence increasing the population of open enzymes and the catalytic turnover in the degradation of small substrates.[11] However, there is no consensus in the mechanism by which ATP inhibits the enzyme in the case of long substrates.[24,26−29] Understanding the regulation mechanism is challenging and will help in the development of new therapies against AD.

Motivated by recent discoveries and the social impact of AD,[30] we have investigated the regulatory mechanism of IDE in breakdown of Aβ42 by ATP. Recently, on the basis of the results of extensive molecular dynamics (MD) calculations of IDE bound to Aβ42 in the absence or presence of ATP, we have proposed a molecular model for this inhibition.[27] Our model ATP, which is bound to IDE-C, interacts with Aβ42 bound to the opposite half (IDE-N), creating a link that connects the two halves of IDE trapping the enzyme in the closed (inactive) conformation and ultimately inhibiting its catalytic function. We also observed that ATP induces geometric changes in the active site, which can be related to the destabilization of the reaction intermediates, negatively impacting the reaction kinetics. In the present article, we follow up on this study by investigating the reaction mechanism of amyloid degradation by IDE in the absence and presence of ATP utilizing an all-atom model of IDE, using umbrella sampling with hybrid quantum mechanics and molecular mechanics (QM/MM) simulations to generate free energy surfaces for the reactions. The results indicate that the rate-determining step (RDS) has activation free energy equal to 15 ± 2 kcal mol^{-1} in the absence of ATP and becomes 7 kcal mol^{-1} higher in the presence of ATP. Thus, the presence of the nucleotide increases the rate constant by a factor of 10^5.

METHODOLOGY

The initial structures of Aβ42−IDE systems in the absence and presence of ATP were obtained from our previous study.[27] Briefly, the initial IDE structure was obtained from the Protein Data Bank (PDB) (PDB ID: 2WK3). The protonation states of ionizable residues were determined by MolProbity.[31] Residues that were not visible in X-ray diffraction were added using SwissView.[32] Aβ42 was docked in IDE using AutoDock[33,34] with the Aβ42 residues which were detectable by X-ray diffraction fixed in the experimental position. Starting from this last structure and docking ATP at the cationic site, the IDE−Aβ42+ATP system was built. All systems were solvated with TIP3P water molecules,[35] and each system was simulated by molecular dynamics for over 40 ns. In both cases, the nitrogen atoms in HIS108 and HIS112, the two oxygen atoms of the carboxyl group in GLU189, and the carbonyl oxygen phe19 and reactive oxygen of the water molecule coordinate to the Zn^{2+} ion to form the first coordination shell. [For clarity, in this text we use uppercase three-letter symbols for IDE residues and lowercase for amyloid residues.] IDE residues GLU111, GLU182, THR220, ARG824, and TYR831 form the second

DOI: 10.1021/ci500544c
J. Chem. Inf. Model. 2015, 55, 72−83

Scheme 1. Reaction Mechanism for Amyloid Degradation by IDE

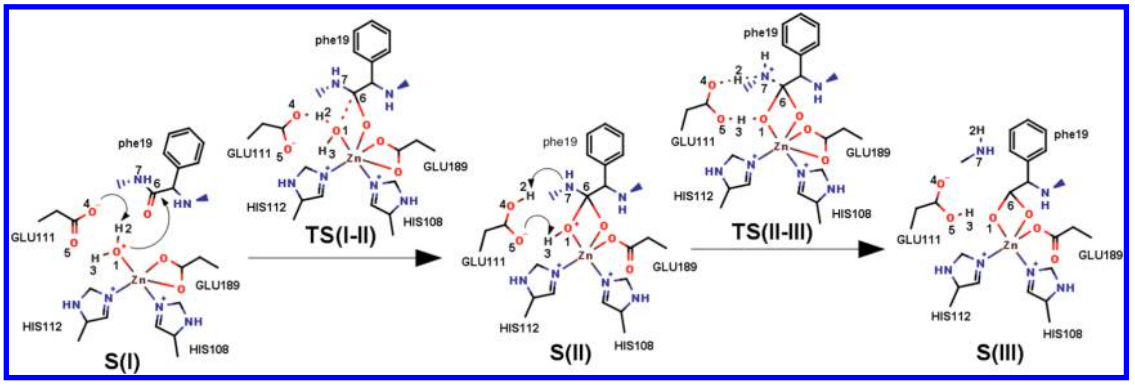

coordination shell and are known to play a key role in the recognition, binding, and breaking of the substrate and stabilization of the active site structure of the process.[36,37] GLU111 participates in the catalytic process by assisting in the H2 proton transfer from O1 to N7, while the side chains ARG824 and TYR831 help in fixing the substrate and stabilizing the reaction structures. The amino group of ARG824 interacts with phe20 carbonyl oxygen, and the hydroxyl group TYR831 interacts with the carbonyl oxygen of phe19. In our previous simulations, these interactions are observed in the absence and presence of ATP except for the last one, which is broken in the presence of ATP as shown in Figure 2. In this case, the population of hydrogen bonds TYR831−phe19 is reduced, while a hydrogen bond is formed TYR831−ala21.[27] From each of the trajectories generated (with and without ATP), one structure was chosen with the requirements that (a) those interactions are reproduced and (b) the reaction coordinates had values close to the starting point in the umbrella sampling path (see below).

In the QM/MM scheme used here, the system was divided into a QM and MM region.[38,39] The QM region consisted of the two Aβ42 residues involved in the bond breaking (phe19 and phe20), active site residues (HIS108, HIS112, GLU189, and Zn^{2+}), catalytic amino acid GLU111, and zinc-bound water molecule. To reduce the boundary effects, the val18 α-carbon and ala21 nitrogen were added to the QM region. Link hydrogen atoms were added to complete the valence of the atoms of the QM system, totaling 120 QM atoms (Figure 3). The rest of the system (MM region) consisted of over 66,000 atoms. The energy of the QM region was calculated using the self-consistent charge density-functional tight-binding method (SCC-DFTB),[40] and the remainder of the system was treated with the AMBER force field FF99SB.[41] SCC-DFTB is an approximate method based on the formalism of density functional theory (DFT) and which has been shown to provide accurate structural and energetic properties for biological systems.[42−46] This method has been adapted to simulate zinc metalloproteases[47] and since then has been successfully used to study β-lactamases,[48−52] peptidases,[53−56] phosphatases,[57] and carbonic anhydrase.[58] Corrections have been included to account for the presence of hydrogen bonds.[45,59] The SCC-DFTB method is implemented in the AMBER package for simulation of biological molecules.[60,61]

The reactions in the absence and presence of ATP were simulated by using umbrella sampling to steer the distances between the atoms involved in the formation of the chemical bonds—C6−O1 [r(O1−C6)] and N7−H2 [r(N7−H2)]—and the weighted histogram analysis method (WHAM) to reconstruct the potential of mean force (PMF) from the results. This method has been extensively used and reviewed before, including for zinc metalloproteases.[49,52−57,62] No control was imposed upon other atoms. The complete free energy surface resulting from the choice of these two coordinates was calculated sweeping all possible combinations of r(O1−C6) and r(N7−H2). In all steps, a force constant was used to restrain the reaction coordinated to the window center. Two types of windows were used. Near the energy minima (reactants, intermediates, and products) a spacing of 0.2 Å between windows was used, combined with a weak restraint of 400 kcal mol^{-1} $Å^{-2}$, and a tighter spacing of 0.1 Å with a stronger restraint of 800 kcal mol^{-1} $Å^{-2}$ for windows closer to critical (transition) states, totaling 68 windows for each reaction.

Apart from the initial structures obtained as described above, the initial geometry of each successive umbrella window was obtained starting from the neighbor window with reaction coordinate values closest to the new one. In all cases, the initial structure was subjected to 1000 cycles of steepest descent geometry optimization while keeping only the reaction coordinates restrained to the desired value and allowing all other atoms to move. After the initial minimization, the constraints were maintained, and the structure for each window was continuously heated at a constant volume from 0 to 300 K for 3 ps, with 0.5 fs time step. Then each window was simulated at a constant 300 K temperature and 1 atm pressure for 22.0 ps with a 1.0 fs time step, totaling 25 ps of simulation. Together, these calculations add up to 3.4 ns simulation with and without ATP. The electrostatic and van der Waals interactions used a cutoff radius of 12.0 Å, and the long-range interactions were treated with the particle mesh Ewald method (PME).[63] The temperature was controlled using a Langevin thermostat with collision frequency of 2.0 ps^{-1},[64] and the pressure was controlled using the Beredensen barostat with 2.0 ps relaxation time.[65]

All analyses considered only the final 15.0 ps of each simulation. Calculations were performed with the Sander program, and the results treated with ptraj and ccptraj programs, both part of the molecular dynamics simulation package AMBER12.[61] The PMF was reconstructed from the dynamics of windows using Alan Grossfield's WHAM program, with a tolerance of 0.0001 in the (dimensionless) free energy.[66]

RESULTS

The reaction mechanism considered is shown in Scheme 1. The complete free energy surfaces obtained with the two-dimen-

DOI: 10.1021/ci500544c
J. Chem. Inf. Model. 2015, 55, 72−83

sional scans of the C6−O1 and N7−H2 coordinates, in the absence and presence of ATP, are shown in Figure 4, and the

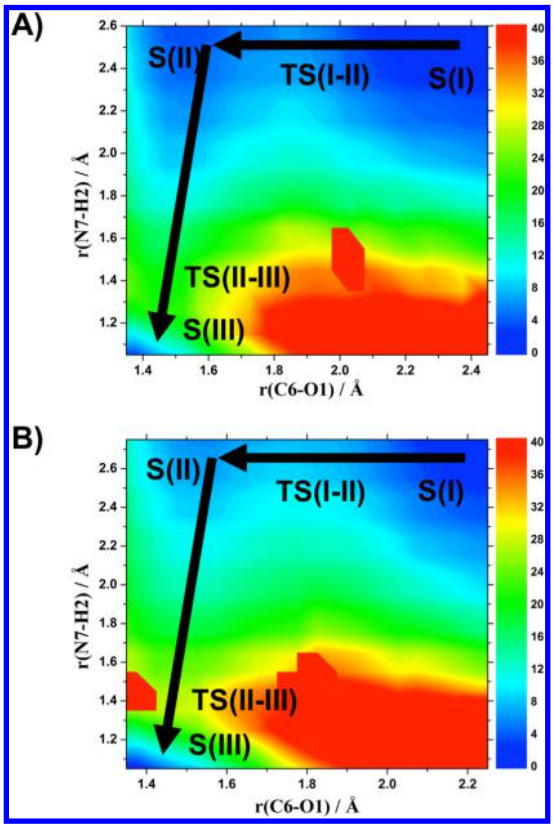

Figure 4. Free energy surfaces for the amyloid degradation reactions by IDE in the absence (A) and presence (B) of ATP. The arrows indicate the least energy pathway, and the labels correspond to the structures in Scheme 1.

reaction profiles following the path of least energy are alternately displayed in Figure 5. The relative energies for each important structure are shown in Table 1. Tridimensional structures representing the reactants, intermediates, transition state, and reaction products are shown in Figure 6 for the reaction in the absence of ATP and in Figure 7 for the reaction in the presence of ATP. The function of THR142 in the

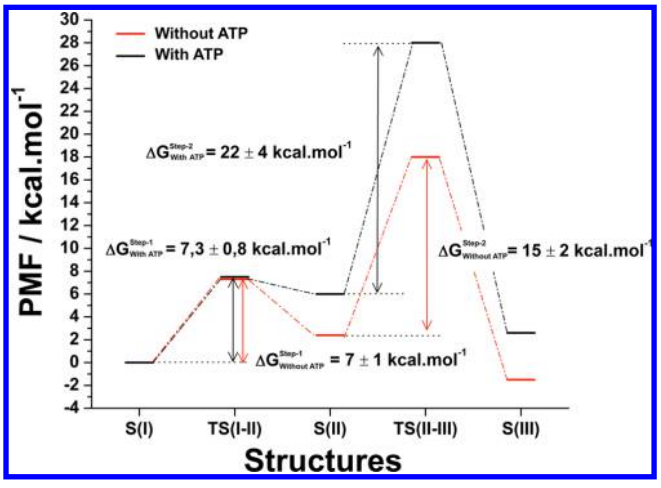

Figure 5. Free energies profiles for the reactions in the absence (red) and presence (black) of ATP.

Table 1. Relative Free Energies for Various Structures in the Reaction Path

structure	without ATP (kcal mol^{-1})	with ATP (kcal mol^{-1})
S(I)	0	0
TS(I−II)	7 ± 1	7.3 ± 0.8
S(II)	2 ± 1	6 ± 2
TS(II−III)	17 ± 2	28 ± 4
S(III)	−1.8 ± 0.8	2 ± 0.8

reaction mechanism was also investigated by evaluating in terms of hydrogen bonds, which is shown in Table 2. Finally, the effect of ATP on the structure around the active site is shown in Figure 8 and the effect on the charge is shown in Figure 9. Finally, the effect of the catalytic center hydration was evaluated calculating the average number of molecules of water that appears next to 5.0 Å away from the zinc during the 40 ns simulation of molecular dynamics without and with ATP, as shown in Figure 10.

DISCUSSION

Reaction Mechanism in Absence of ATP. The reaction mechanism of IDE in the degradation of insulin was first studied computationally by Amata et al. in 2009.[67] In that study, the enzyme was represented by a cluster model of the active site containing 130−159, and the DFT/B3LYP level of theory with implicit solvent was used to simulate the reaction. They obtained a three-step reaction mechanism where GLU111 has a function of activating the Zn-bound water molecule. The first step, comprising the water oxygen attack to the substrate carbonyl carbon, happens through a transition state similar to TS(I−II) considered here. The second step is a rearrangement leading to the formation of the gen-diol intermediate, S(II), and the third step leads to the products. The rate-determining step of the reaction was determined to be the first, with activation energy of 15.6 kcal mol^{-1}. Less than two months later, Bora et al. submitted a paper reporting a DFT/B3LYP study on the reaction of Aβ42 degradation by IDE.[68] In these studies, the authors considered only the main amino acids involved in reaction, which were the triad of amino acids bonded to zinc, the water molecule bound to the metal, the catalytic amino acid GLU111, the Zn ion, and the phe19−phe20 pair of residues, whose peptide bond will be broken. To mimic the enzyme environment, implicit solvent with a dielectric constant of 4.3 (corresponding to ether) was used, along with positional constraints to the α-carbons to hold the geometry in the crystallographic position. No other amino acid around the active site was considered in this approach. Their results pointed that degradation would occur in three steps. The first step is the activation of the water molecule by GLU111 and attack of the carbonyl carbon of the scissile bond. The second step is the formation of the gen-diol intermediate. The third and last step results in breaking the substrate's peptide bond. The rate-determining step of the reaction was the first step, with activation energy equal to 16.6 kcal mol^{-1}. The following processes would occur with activation energies below 10.0 kcal mol^{-1}.

In our simulations, the full enzymatic environment was considered explicitly, and the reaction follows a similar mechanism but with a somewhat different energy profile. Water activation occurs concurrently with the attack of carbon C6 by oxygen O1, leading directly to the formation of the gen-diol intermediate, with activation energy around 7 ± 1 kcal

DOI: 10.1021/ci500544c
J. Chem. Inf. Model. 2015, 55, 72−83

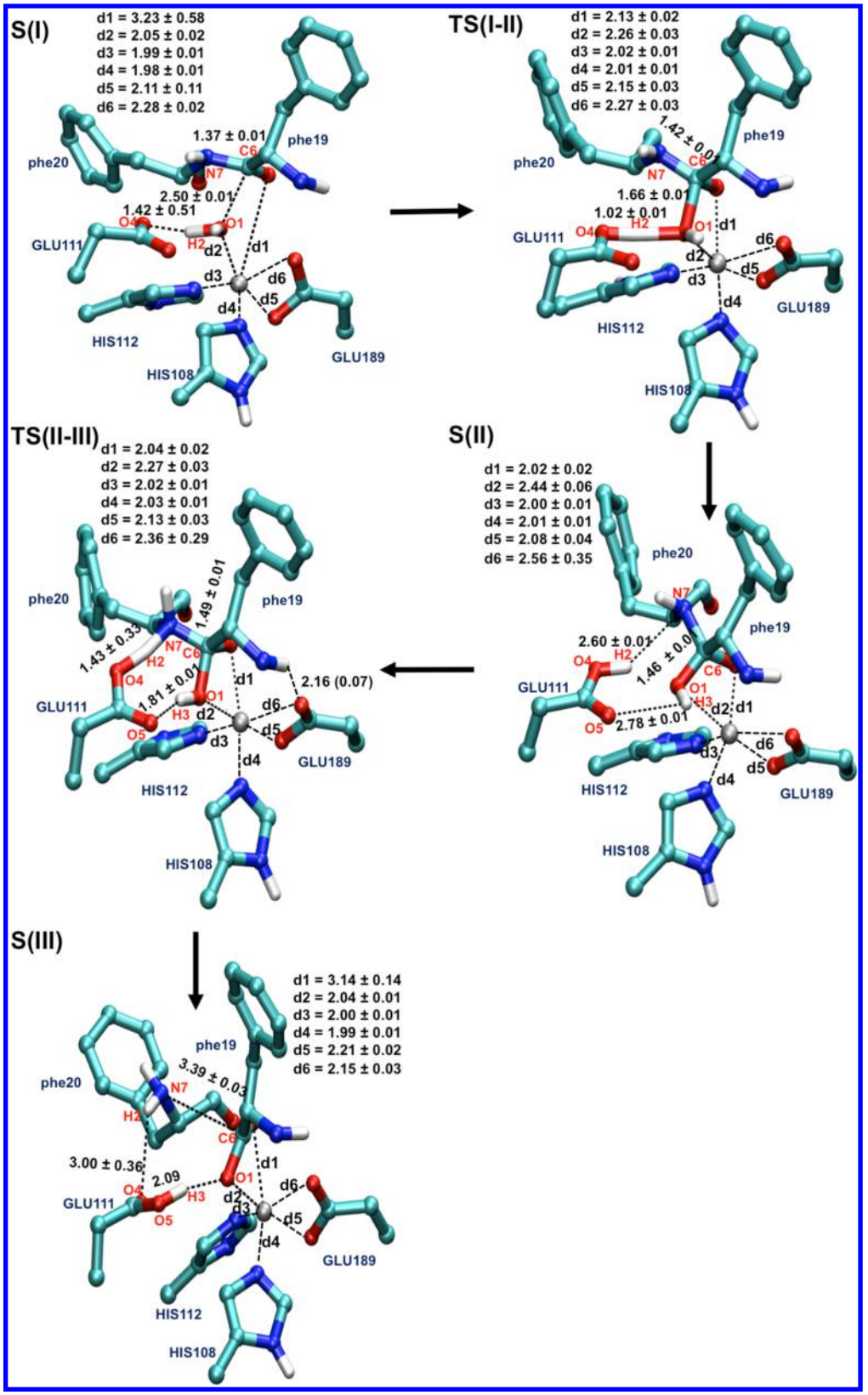

Figure 6. Details of the reaction structures in the absence of ATP.

mol^{-1} in the absence of ATP. The following processes occur simultaneously leading to the breaking of the peptide bond, with activation energy equal to 15 ± 2 kcal mol^{-1}, being therefore the rate-determining step. The difference in the results reflects the importance of an atomistic description of the molecular environment on the determination of the energy profile for enzymatic reactions. The reaction mechanism obtained in our simulations is similar to the reaction of termosilin, a metalloprotease from the same family as IDE, reinforcing the results presented here.[69] The important catalytic

DOI: 10.1021/ci500544c
J. Chem. Inf. Model. 2015, 55, 72−83

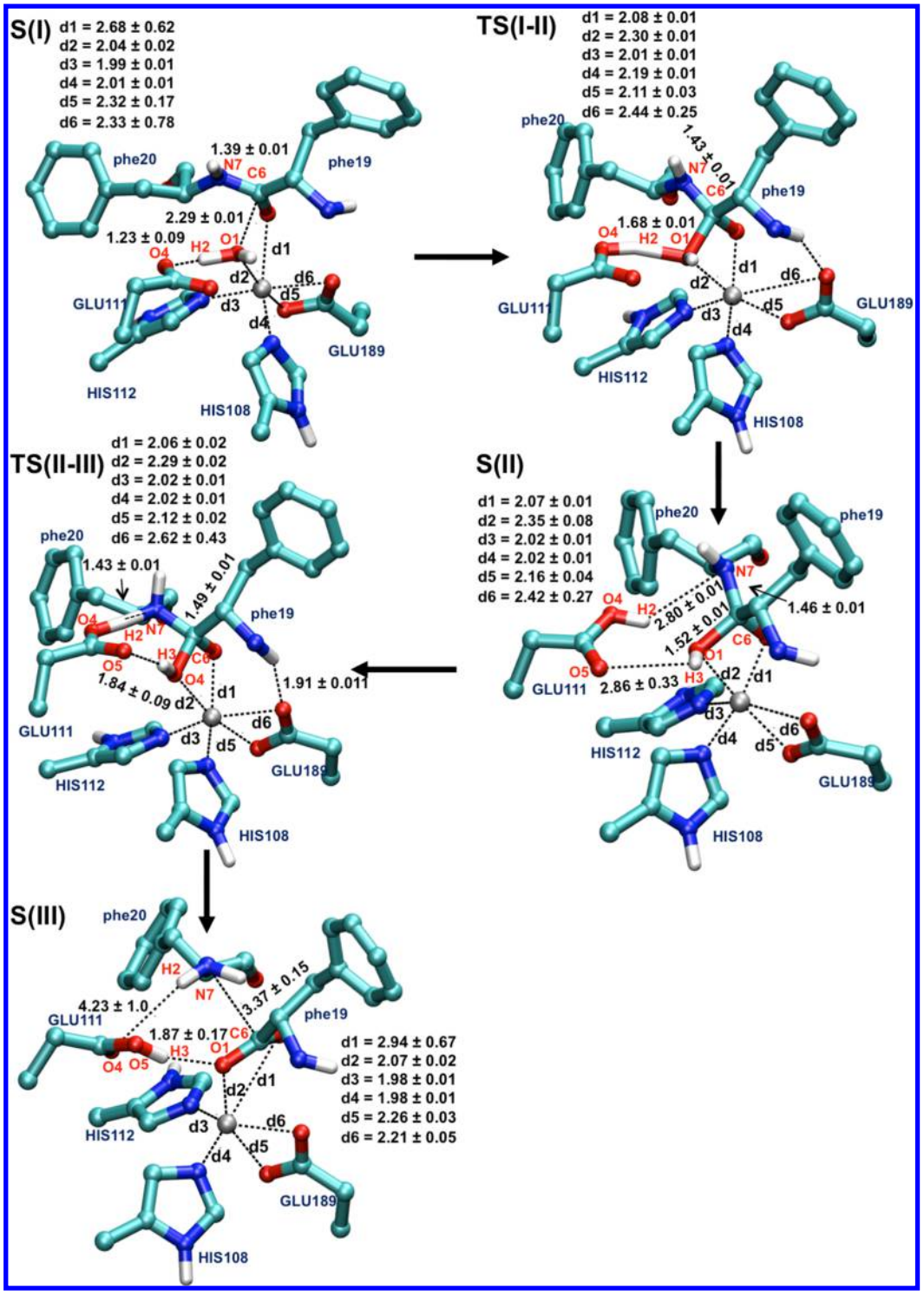

Figure 7. Details of the reaction structures in the presence of ATP.

function of GLU111 was confirmed in our studies, as well as THR142 role for the stabilization of the carboxylic oxygen GLU111.

It is shown from the free energy surfaces in Figure 4 and the profiles in Figure 5 that the path of least energy for the reaction in the absence of ATP is consistent with a reaction of two steps. Step 1 is represented by a reduction of the coordinate r(C6−O1) and concerns activation of the reactive water and formation of the gen-diol intermediate. Step 2 is represented by a reduction in the r(N7−H2) coordinate, leading to breakage of the substrate's peptide bond. In the first step, the carboxylic oxygen GLU111 (O4) abstracts a proton from the reactive water (H2) at the same time that the oxygen from the same water molecule (O1) attacks the carbonyl carbon of phe19 (C6) leading, through transition state TS (I−II), to the intermediate S(II), as shown in Scheme 1. Note that the first attack is not controlled in our simulations and happens spontaneously while we drive the second using the bias potential. In the next step, the GLU111 donates the proton captured in the previous step to nitrogen of phe20 (N7), while

DOI: 10.1021/ci500544c
J. Chem. Inf. Model. 2015, 55, 72−83

Table 2. Occupancy of GLU111−THR142 Hydrogen Bond (percentage of total of frames) at Various Structures[a]

structure	occupancy (%)
S(I)	78
TS(I−II)	51
S(II)	52
TS(II−III)	28
S(III)	31

[a]A H-bond was considered when the distance between donor and acceptor atoms was inferior to 3.0 Å and the donor−hydrogen−acceptor angle was greater than 110° [84] (Figure 2).

the H3 proton is abstracted by GLU111 carboxylic oxygen (O5). The phe19−phe20 peptide bond (C6−N7) is broken, leading to the reaction product S(III) through the transition state TS(II−III).

In the absence of ATP, the initial structure presents the zinc atom coordinated to a water molecule, two histidines (HIS108 and HIS112), and glutamate (GLU189) through bonds d2, d3, d4, d5, and d6, being 2.05 ± 0.02, 1.99 ± 0.01, 1,98 ± 0.01, 2.11 ± 0.11, and 2.28 ± 0.02 Å in length, respectively, forming a zinc complex penta-coordinated S(I), as shown in Figure 6. The substrate is disconnected from the active site, as shown by the distance between the oxygen phe19 of the substrate and ion active site Zn^{2+} (d1) of 3.23 ± 0.58 Å. During the first step, the substrate approaches the catalytic center with reduction of the r(C6−O1) distance from 2.50 ± 0.01 Å in S(I) to 1.66 ± 0.01 Å in TS (I−II), promoting the formation of a bond between the phe19 oxygen and the Zn^{2+} ion (d1), being 2.13 ± 0.02 Å in length in the transition state. The metal polarizes and weakens the C6−N7 bond, which can be seen by its elongation from 1.37 ± 0.01 Å in S(I) to 1.42 ± 0.01 in TS(I−II). The transition state TS(I−II) is octahedral around the Zn^{2+} ion and forms with activation energy 7.3 ± 0.8 kcal mol^{-1}. At the same

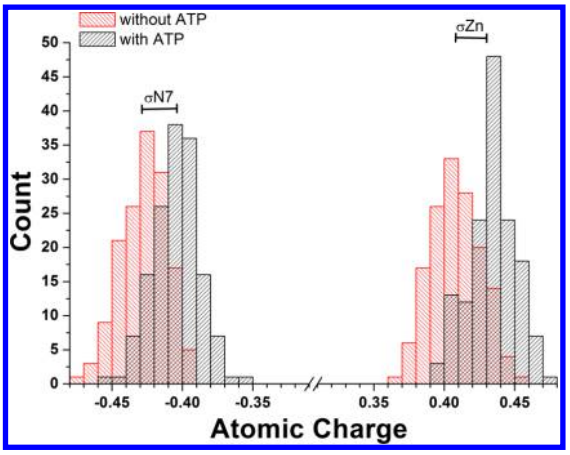

Figure 9. Distribution of atomic (Mulliken) charges on the Zn and N7 atoms in the reaction intermediate S(II) for the systems in the absence (red) and presence (black) of ATP.

time, the GLU111 oxygen O4 moves spontaneously toward the hydrogen H2, suggesting that the nucleophilic attack and the proton abstraction occur synchronously. At this point, the formation of a metastable intermediate is imminent. Then, with the further reduction of r(C6−O1) to 1.46 ± 0.01 Å, the C6−O1 bond is formed, and the H2 proton is completely transferred to the GLU111, reaching an energy minimum in S(II), being 2.4 ± 0.1 kcal mol^{-1} above the reactant's energy. During this process, GLU189 recedes as the d6 bond is elongated from 2.27 ± 0.03 to 2.56 ± 0.35 Å, forming the penta-coordinated metastable intermediate S(II).

In step 2, the H2 proton transfer from GLU111 to phe19's N7 is steered by decreasing the r(N7−H2) coordinate from 2.66 Å in S(II) to 1.43 Å in TS(I−II). During the transfer, GLU111's oxygen O5 spontaneously aligns with the remaining

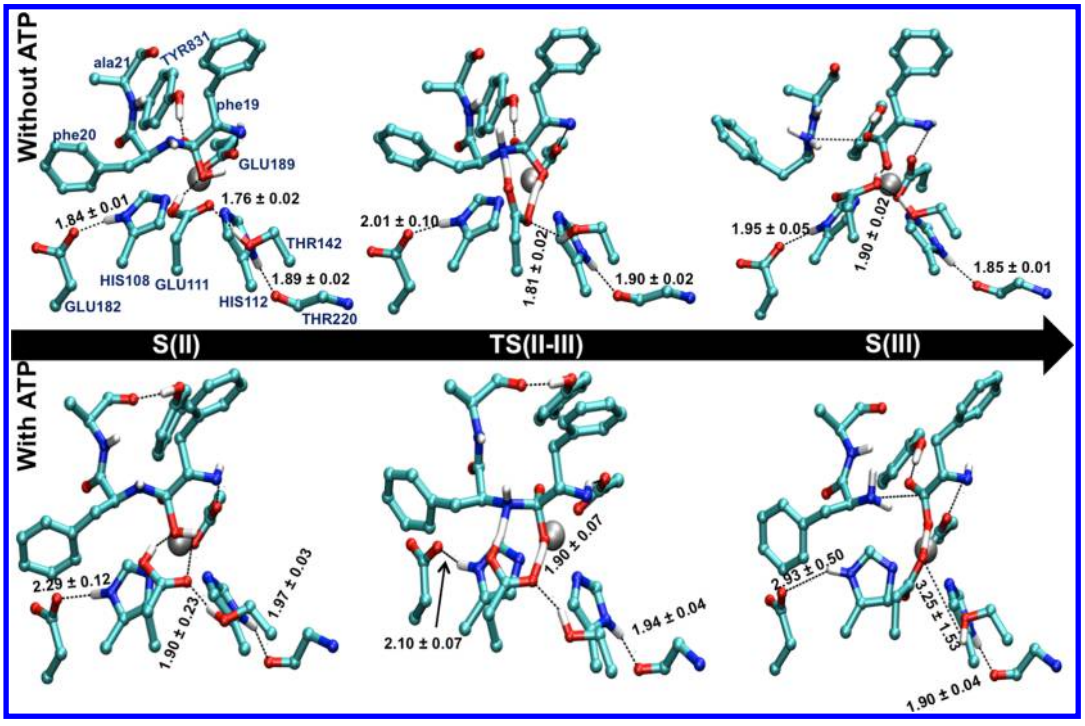

Figure 8. Main interactions of residues from the second coordination shell with residues from the first coordination shell around the Zn atom in step 2 (rate-determining step) in the absence (top) and presence (bottom) of ATP.

DOI: 10.1021/ci500544c
J. Chem. Inf. Model. 2015, 55, 72−83

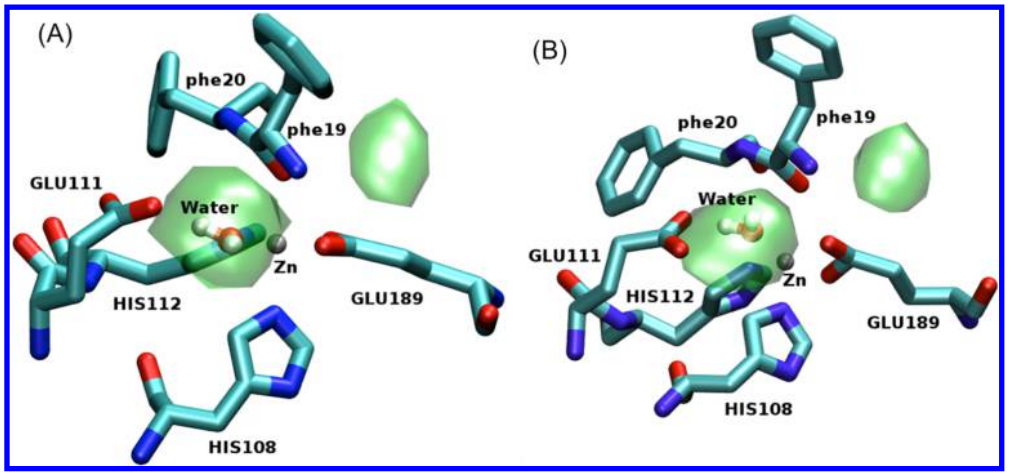

Figure 10. Water occupation map on the region within 5.0 Å from the Zn atom: (A) in the absence of ATP and (B) in the presence of ATP. Generated by VolMap (VMD) using a isovalue of 1.0.

hydrogen (H3) from the reactive water molecule (H3−O5 distance 2.78 ± 0.01 Å), suggesting that the H2 proton transfer and H3 hydrogen capture occur synchronously. As the N7−H2 distance is reduced, polarization increases, and the substrate peptide bond (C6−N7) weakens, which is represented by the slight increase from 1.46 ± 0.01 Å in S(II) to 1.49 ± 0.01 Å in TS(II−III). The distance d6 is reduced to 2.36 ± 0.29 Å, favoring the formation of the hexa-coordinated transition state, with an activation energy of 15 ± 2 kcal mol^{-1}. Finally, the H2 proton is completely transferred to the N7 nitrogen atom, and the H3 hydrogen is captured by GLU111, resulting in breakage of the peptide bond (C6−N7) and formation of the reaction products S(III). The lowest energy level is reached at this point, with Gibbs free-energy (ΔG) 1.5 ± 0.6 kcal mol^{-1} below the reactants, indicating that the enzymatic reaction is spontaneous and thermodynamically favorable. This last step of the reaction has the highest activation barrier and is therefore the rate-determining step of the reaction (Table 1).

Comparison to Experimental Kinetic Rates. The rate of degradation of Aβ by IDE has been determined by Leissring using two different methods, fluorescence polarization (FP) and avidon-agarose precipitation (AAP), with a derivatized Aβ peptide of the fluorescein-Aβ-(1−40)-Lys-biotin. Both methods resulted in very similar results, with a k_{cat} of 256 ± 22 min^{-1}(FP) and 221 ± 11 min^{-1} (AAP).[70] Assuming first-order kinetics and transition state theory with unity transmission coefficient, those values correspond to an activation free energy barrier between 16.5 and 16.7 kcal mol^{-1}, in perfect agreement with our calculated activation energy (Table 3).

Table 3. Activation Energy of Rate-Determining Step of the Reaction and Kinetic Rate Constant Calculated at 300 K

system	$\Delta G^{\ddagger}_{TS(II-III)}$ (kcal mol^{-1})	k_R (s^{-1})
without ATP	15 ± 2	10^5
with ATP	22 ± 4	1

Role of GLU111. During the reaction, the essential function of GLU111 in the proton transfer from the reactive water to the substrate became evident, initially as a base to abstract the proton from water and subsequently as acid to deliver the proton to the substrate's nitrogen. Thus, we also evaluated the GLU111 interactions with neighboring residues. In the crystal structure, as in the initial structures, the carboxylic GLU111 oxygen interacts with the hydrogen of the hydroxyl THR142 via hydrogen bonding (GLU111−THR142). However, this bond is broken during the reaction. Table 2 shows the occurrence of this interaction in the reactant S(I), intermediate S(II), and S(III) product. The bond is more present in S(I) when GLU111 acts as a base than in S(II) when it acts as acid, suggesting that the GLU111−THR142 hydrogen bond is responsible for stabilizing the carboxylic group GLU111 for the first step of the reaction.

Hydration of the Active Site. Previous studies have shown that in a similar reaction in β-lactamases consideration of a second water molecule as suggested by MD simulations but not seen in the experimental structures considerably lowers the activation energy and was necessary to reproduce experimental kinetic rates.[71,72]

We have examined this possibility in the case of IDE. In our molecular dynamics simulations,[73] the average number of waters around the active site is 1.3 and 1.4 for systems without and with ATP, respectively, indicating that a second water molecule does periodically approach the active site. Examining the population map around the active site (Figure 10), one notices that this second water molecule is located further away and is unable to participate in the reaction. Moreover, the currently considered mechanism already reproduces the experimental reaction kinetics,[74] and the consideration of the alternative mechanism is not warranted, as no participation of a second water molecule has been suggested in any of the previous theoretical or experimental results.[37,74−76]

ATP Effect in the Reaction Mechanism. Similar to the reaction in the absence of ATP, the structure of the reagent in the presence of ATP also shows a penta-coordinated complex, with the zinc ion bound to a water molecule, two histidines, and a glutamate, as shown in Figure 7. The reaction mechanism is similar to the reaction without ATP but with significant changes in the energy of the first intermediate and geometry of the transition states, especially in TS(II−III), and consequently on the reaction energies.

It is shown from Table 1 that in the presence of ATP intermediate S(II) is now energetically indistinguishable from TS(I−II) within error bars, indicating that this structure is destabilized in the presence of ATP. In the formation of the second transition state, the d6 bond is broken with increasing the distance from 2.42 ± 0.27 Å in S(II) to 2.62 ± 0.43 Å in TS(II−III), while the hydrogen bond between the carboxyl

DOI: 10.1021/ci500544c
J. Chem. Inf. Model. 2015, 55, 72−83

oxygen from GLU189 and the amino hydrogen in phe19 is formed, leading to a penta-coordinated transition state TS(II−III), in contrast to the hexa-coordinated TS(II−III) found in the absence of the nucleotide. The new arrangement destabilizes the TS, resulting in an increase in the activation barrier of step 2 from 15 ± 2 to 22 ± 4 kcal mol^{-1} as shown in Figure 5. In terms of reaction kinetics, this represents a reduction in the rate constant in the order of 10^5 times. A similar effect has been observed by Wu et al. after catalytic removal of acetyl groups from the histone tails of histone deacetylase enzyme zinc-dependent 8 (HDA8), with a K^+ ion located about 7.0 Å away from the catalytic Zn^{2+} ion.[77] In this study, the presence of the ion modifies the charge distribution of the active site, making it a less efficient enzyme.

From a structural perspective, the ATP−substrate interaction induces changes in the active site geometry that affect the amyloid binding to the catalytic site region, as shown in Figure 8. The decrease in the TYR831−phe19 incidence and the formation of the TYR831−ala21 interaction, the latter detected only in the presence of ATP, increases the flexibility of the substrate's phe19, interfering with the Zn−substrate binding mode. In turn, loss of the TYR831−phe19 interaction destabilizes S(II) and favors the change in the zinc coordination of TS(II−III) from hexa-coordinated in the absence of ATP to penta-coordinated in the presence of ATP, also destabilizing the TS and leading to an increase in the activation energy of the rate-determining step of the reaction. The TYR831−phe19 interaction is restored in the product. In addition to this interaction, in the presence of ATP, the distances HIS108−GLU182 and GLU111−THR142 in S(III) are stretched to near 3.0 Å, effectively breaking these interactions and contributing to the destabilization of the active site structure.

The atomic charges on the Zn ion and N7 work are in a delicate balance to allow the H3 abstraction from the water by GLU111 and the H2 transfer to N7. In principle, the positive charge of the Zn ion should polarize and weaken the O1−H3 and C6−N7 bonds, contributing respectively to the H3 proton abstraction by GLU111 and degradation of the substrate, making Zn a Lewis acid. At the same time, the negative charge on the N7 atom should act as a general base to accept the H2 proton from GLU111, making the N7 atom an important Lewis base. Therefore, the more positive the Zn charge is, the more powerful a Lewis acid it becomes to activate the reactive water. On the other hand, the more negative charge on the N7 atom makes it a stronger Lewis base to abstract the H2 proton from GLU111. We investigated the Mulliken charges on these atoms in the S(II) intermediate, which are shown in Figure 9. The results show that in the presence of ATP the Zn charge is increased, facilitating the H3 abstraction by GLU111. However, the charge on N7 is reduced, making it a less effective Lewis base and impairing the H2 to N7 proton transfer needed to form the reaction products. This breaking of the charge balance contributes to destabilize S(II) and increase the activation energy needed to form TS(II−III).

Mechanism of IDE Inhibition by ATP. Experimental studies show that the rate constant for IDE reaches values up to 2500 s^{-1} in the degradation of small peptides such as bradykinin and kallidin.[74] However, for long substrates such as insulin, it can be as small as about 0.56 min^{-1}.[78,79] Binding of a large substrate requires a higher level of organization than a small substrate. To connect to IDE, a large substrate must interact initially with the distal site and subsequently with the active site. Moreover, two molecules of a small substrate are directly connected to the distal and each active site, producing the same activating effect of a large substrate−symmetrical homotropic allosteric activation.[80,81] It is reasonable to assume that the time scale to the opening-and-closing movement of the enzyme is similar in both cases, and the difference is only in the recognition and binding time of the substrate. Therefore, the recognition time in this case determines the efficiency of the IDE.

Moreover, contradictory effects are observed in the presence of ATP, which works as an activator in the degradation of small substrates, and IDE inhibitor in the degradation of long substrates.[24,82] The presence of the nucleotide eliminates the symmetric allosteric activation with the change of IDE quaternary structure from dimers to monomers but displays an allosteric activation mechanism sequence that prioritizes open conformation of IDE only during proteolysis of a small substrate.[29] According to the authors, ATP binds to the cationic site located on the IDE-C, breaking the charge balance between the two halves of the enzyme, a complementary pattern established by the charge distribution of IDE-C (positive) and IDE-N (negative). The weakening of the electrostatic force holding the halves of the IDE in the closed conformation culminates in increasing the proportion of open (active) enzyme state and the enhancement of the catalytic power. In the case of a long substrate, our previous molecular dynamics simulations suggest that ATP interacts with the C-terminal tail of the substrate by creating a bridge that connects and holds the halves of the enzyme in the closed conformation and induces structural changes in the active site, which were hypothesized to lead to a proteolytically inappropriate configuration.[27] In the present study, this hypothesis was verified by comparing the reaction profiles in the presence and absence of ATP, which clearly showed an increased activation barrier in the presence of ATP.

In principle, two factors could contribute to the changes in the reaction profile in the presence of ATP: (1) loss of the TYR831−phe19 interaction, observed in the previous study, and/or (2) unbalanced charges in the catalytic center. The large distance between the ATP and the metal center (about 18 Å) puts it out of range for nonbonded interactions, thus eliminating the effect of the ATP charge. However, the results still show significant changes in the Zn and N7 charges, indicating that the presence of ATP still influences the charge distribution of QM region, likely by forcing a different atomic arrangement around it. Moreover, the loss of the TYR831−phe19 interaction in the presence of ATP, important for fixation and recognition of the substrate, and the stabilization of the catalytic reaction intermediates[36,83] changes the coordination structure around the catalytic center to a less favored structure, reducing the reaction rate in about 10^5 times.

These results support the hypotheses in our previous article that the presence of ATP forms a new IDE−ATP, ATP−substrate, and substrate−IDE sequence of interactions responsible for holding IDE in the closed (inactive) conformation and induces conformational changes in the active site region leading to a proteolytically inefficient configuration, ultimately reducing the rate of amyloid degradation.

CONCLUSION

To our knowledge, this is the first study to determine the energy profile for the mechanism of degradation of Aβ42 by IDE considering the complete enzyme environment in the presence of ATP. According to our results, the reaction occurs

DOI: 10.1021/ci500544c
J. Chem. Inf. Model. 2015, 55, 72−83

in two steps. The first step involves the water activation and formation of a gen-diol complex. The second step leads to the breaking of the peptide bond, the latter being the rate-determining step of the reaction with activation energy equal to 15 ± 2 kcal mol^{-1}, in perfect agreement with available experimental kinetics data.[76]

The presence of ATP induces structural changes in the substrate leading to a proteolytically inefficient configuration around the active site, increasing the activation energy of the rate-determining step in about 7 kcal mol^{-1} and in turn reducing the catalytic constant of the reaction by a factor of around 10^5, determining enzyme inactivation.

AUTHOR INFORMATION

Corresponding Author

*E-mail: gustavo.seabra@ufpe.br.

Notes

The authors declare no competing financial interest.

REFERENCES

(1) Saido, T. C. *Aβ Metabolism and Alzheimer's Disease*; Saido, T. C., Ed.; Eurekah.com/Landes Bioscience: Georgetown, Texas, 2003.

(2) Iwata, N.; Higuchi, M.; Saido, T. C. Metabolism of Amyloid-Beta Peptide and Alzheimer's Disease. *Pharmacol. Ther.* **2005**, *108*, 129−148.

(3) Hardy, J.; Higgins, G. Alzheimer's Disease: The Amyloid Cascade Hypothesis. *Science* **1992**, *256*, 184−185.

(4) Minati, L.; Edginton, T.; Bruzzone, M. G.; Giaccone, G.; Grazia Bruzzone, M. Current Concepts in Alzheimer's Disease: A Multidisciplinary Review. *Am. J. Alzheimers Dis. Other Demen.* **2009**, *24*, 95−121.

(5) Schenk, D.; Barbour, R.; Dunn, W.; Gordon, G.; Grajeda, H.; Guido, T.; Hu, K.; Huang, J.; Johnson-Wood, K.; Khan, K.; Kholodenko, D.; Lee, M.; Liao, Z.; Lieberburg, I.; Motter, R.; Mutter, L.; Soriano, F.; Shopp, G.; Vasquez, N.; Vandevert, C.; Walker, S.; Wogulis, M.; Yednock, T.; Games, D.; Seubert, P. Immunization with Amyloid-Beta Attenuates Alzheimer-Disease-like Pathology in the PDAPP Mouse. *Nature* **1999**, *400*, 173−177.

(6) Chen, G.; Chen, K. S.; Knox, J.; Inglis, J.; Bernard, A.; Martin, S. J.; Justice, A.; Mcconlogue, L.; Games, D.; Freedman, S. B.; Morris, R. G. M. A Learning Deficit Related to Age and Beta-Amyloid Plaques in a Mouse Model of Alzheimer's Disease. *Nature* **2000**, *2940*, 975−979.

(7) Chu, J.; Lauretti, E.; Craige, C. P.; Praticò, D. Pharmacological Modulation of GSAP Reduces Amyloid-B Levels and Tau Phosphorylation in a Mouse Model of Alzheimer's Disease with Plaques and Tangles. *J. Alzheimers. Dis.* **2014**, 140105.

(8) Phiel, C. J.; Wilson, C. A.; Lee, V. M.-Y.; Klein, P. S. GSK-3alpha Regulates Production of Alzheimer's Disease Amyloid-Beta Peptides. *Nature* **2003**, *423*, 435−439.

(9) Song, E.-S.; Juliano, M. A.; Juliano, L.; Hersh, L. B. Substrate Activation of Insulin-Degrading Enzyme (insulysin). A Potential Target for Drug Development. *J. Biol. Chem.* **2003**, *278*, 49789−49794.

(10) Cabrol, C.; Huzarska, M. A.; Dinolfo, C.; Rodriguez, M. C.; Reinstatler, L.; Ni, J.; Yeh, L.-A.; Cuny, G. D.; Stein, R. L.; Selkoe, D. J.; Leissring, M. A. Small-Molecule Activators of Insulin-Degrading Enzyme Discovered through High-Throughput Compound Screening. *PLoS One* **2009**, *4*, e5274.

(11) Noinaj, N.; Song, E. S.; Bhasin, S.; Alper, B. J.; Schmidt, W. K.; Hersh, L. B.; Rodgers, D. W. Anion Activation Site of Insulin-Degrading Enzyme. *J. Biol. Chem.* **2012**, *287*, 48−57.

(12) Malito, E.; Hulse, R. E.; Tang, W.-J. Amyloid Beta-Degrading Cryptidases: Insulin Degrading Enzyme, Presequence Peptidase, and Neprilysin. *Cell. Mol. Life Sci.* **2008**, *65*, 2574−2585.

(13) El-Amouri, S. S.; Zhu, H.; Yu, J.; Marr, R.; Verma, I. M.; Kindy, M. S. Neprilysin: An Enzyme Candidate to Slow the Progression of Alzheimer's Disease. *Am. J. Pathol.* **2008**, *172*, 1342−1354.

(14) Wang, D.-S.; Dickson, D. W.; Malter, J. S. Beta-Amyloid Degradation and Alzheimer's Disease. *J. Biomed. Biotechnol.* **2006**, *2006*, 58406.

(15) Ciaccio, C.; Tundo, G. R.; Grasso, G.; Spoto, G.; Marasco, D.; Ruvo, M.; Gioia, M.; Rizzarelli, E.; Coletta, M. Somatostatin: A Novel Substrate and a Modulator of Insulin-Degrading Enzyme Activity. *J. Mol. Biol.* **2009**, *385*, 1556−1567.

(16) Iwata, N.; Tsubuki, S.; Takaki, Y.; Shirotani, K.; Lu, B.; Gerard, N. P.; Gerard, C.; Hama, E.; Lee, H. J.; Saido, T. C. Metabolic Regulation of Brain Aβ by Neprilysin. *Science* **2001**, *292*, 1550−1552.

(17) Duckworth, W. C.; Bennett, R. G.; Hamel, F. G. Insulin Degradation: Progress and Potential. *Endocr. Rev.* **1998**, *19*, 608−624.

(18) Lynch, J. A.; George, A. M.; Eisenhauer, P. B.; Conn, K.; Gao, W.; Carreras, I.; Wells, J. M.; McKee, A.; Ullman, M. D.; Fine, R. E. Insulin Degrading Enzyme Is Localized Predominantly at the Cell Surface of Polarized and Unpolarized Human Cerebrovascular Endothelial Cell Cultures. *J. Neurosci. Res.* **2006**, *83*, 1262−1270.

(19) Becker, A. B.; Roth, R. A. Insulysin and Pitrilysin: Insulin-Degrading Enzymes of Mammals and Bacteria. *Methods Enzymol.* **1995**, *248*, 693−703.

(20) Authier, F.; Posner, B.; Bergeron, J. Insulin-Degrading Enzyme. *Clin. Invest. Med.* **1996**, *19*, 149−160.

(21) Farris, W.; Mansourian, S.; Chang, Y.; Lindsley, L.; Eckman, E. a; Frosch, M. P.; Eckman, C. B.; Tanzi, R. E.; Selkoe, D. J.; Guenette, S. Insulin-Degrading Enzyme Regulates the Levels of Insulin, Amyloid Beta-Protein, and the Beta-Amyloid Precursor Protein Intracellular Domain in Vivo. *Proc. Natl. Acad. Sci. U.S.A.* **2003**, *100*, 4162−4167.

(22) Noinaj, N.; Bhasin, S. K.; Song, E. S.; Scoggin, K. E.; Juliano, M. A.; Juliano, L.; Hersh, L. B.; Rodgers, D. W. Identification of the Allosteric Regulatory Site of Insulysin. *PLoS One* **2011**, *6*, e20864.

(23) Manolopoulou, M.; Guo, Q.; Malito, E.; Schilling, A. B.; Tang, W.-J. Molecular Basis of Catalytic Chamber-Assisted Unfolding and Cleavage of Human Insulin by Human Insulin-Degrading Enzyme. *J. Biol. Chem.* **2009**, *284*, 14177−14188.

(24) Camberos, M. C.; Perez, A.; Pérez, A. A.; Udrisar, D. P.; Wanderley, M. I.; Cresto, J. C. ATP Inhibits Insulin-Degrading Enzyme Activity. *Exp. Biol. Med. (Maywood)* **2001**, *226*, 334−341.

(25) Del Carmen Camberos, M.; Cresto, J. C. Insulin-Degrading Enzyme Hydrolyzes ATP. *Exp. Biol. Med. (Maywood)* **2007**, *232*, 281−292.

(26) Song, E. S.; Daily, A.; Fried, M. G.; Juliano, M. A.; Juliano, L.; Hersh, L. B. Mutation of Active Site Residues of Insulin-Degrading Enzyme Alters Allosteric Interactions. *J. Biol. Chem.* **2005**, *280*, 17701−17706.

(27) Da Cruz, C. H. B.; Seabra, G. Molecular Dynamics Simulations Reveal a Novel Mechanism for ATP Inhibition of Insulin Degrading Enzyme. *J. Chem. Inf. Model.* **2014**, *54*, 1380−1390.

(28) Song, E. S.; Juliano, M. A.; Juliano, L.; Fried, M. G.; Wagner, S. L.; Hersh, L. B. ATP Effects on Insulin-Degrading Enzyme Are Mediated Primarily through Its Triphosphate Moiety. *J. Biol. Chem.* **2004**, *279*, 54216−54220.

(29) Song, E. S.; Cady, C.; Fried, M. G.; Hersh, L. B. Proteolytic Fragments of Insulysin (IDE) Retain Substrate Binding but Lose Allosteric Regulation. *Biochemistry* **2006**, *45*, 15085−15091.

(30) *World Alzheimer Report 2012: Overcoming the Stigma of Dementia*; Alzheimer's Disease International: London, 2012; pp 1−80.

(31) Chen, V. B.; Arendall, W. B.; Headd, J. J.; Keedy, D. a; Immormino, R. M.; Kapral, G. J.; Murray, L. W.; Richardson, J. S.; Richardson, D. C. MolProbity: All-Atom Structure Validation for Macromolecular Crystallography. *Acta Crystallogr., Sect. D: Biol. Crystallogr.* **2010**, *66*, 12−21.

(32) Dorman, N. SWISS-MODEL and the Swiss-PdbViewer: An Environment for Comparative Protein Modeling. *Biotechniques* **2012**, *53*, 69.

(33) Morris, G. M.; Huey, R.; Lindstrom, W.; Sanner, M. F.; Belew, R. K.; Goodsell, D. S.; Olson, A. J. AutoDock4 and AutoDockTools4: Automated Docking with Selective Receptor Flexibility. *J. Comput. Chem.* **2009**, *30*, 2785−2791.

DOI: 10.1021/ci500544c
J. Chem. Inf. Model. 2015, 55, 72−83

(34) Morris, G. M.; Goodsell, D. S.; Pique, M. E.; Lindstrom, W.; Huey, R.; Forli, S.; Hart, W. E.; Halliday, S.; Belew, R.; Olson, A. J. AutoDock Version 4.2, 2010, 1−49.
(35) Mahoney, M. W.; Jorgensen, W. L. A Five-Site Model for Liquid Water and the Reproduction of the Density Anomaly by Rigid, Nonpolarizable Potential Functions. *J. Chem. Phys.* **2000**, *112*, 8910−8922.
(36) Shen, Y.; Joachimiak, A.; Rosner, M. R.; Tang, W.-J. Structures of Human Insulin-Degrading Enzyme Reveal a New Substrate Recognition Mechanism. *Nature* **2006**, *443*, 870−874.
(37) Amata, O.; Marino, T.; Russo, N.; Toscano, M. Human Insulin-Degrading Enzyme Working Mechanism. *J. Am. Chem. Soc.* **2009**, *131*, 14804−14811.
(38) Warshel, A.; Levitt, M. Theoretical Studies of Enzymic Reactions: Dielectric, Electrostatic and Steric Stabilization of the Carbonium Ion in the Reaction of Lysozyme. *J. Mol. Biol.* **1976**, *103*, 227−249.
(39) Field, M. J.; Bash, P. A.; Karplus, M. A Combined Quantum Mechanical and Molecular Mechanical Potential for Molecular Dynamics Simulations. *J. Comput. Chem.* **1990**, *11*, 700−733.
(40) Elstner, M.; Porezag, D.; Jungnickel, G.; Elsner, J.; Haugk, M.; Frauenheim, T.; Suhai, S.; Seifert, G. Self-Consistent-Charge Density-Functional Tight-Binding Method for Simulations of Complex Materials Properties. *Phys. Rev. B* **1998**, *58*, 7260−7268.
(41) Hornak, V.; Abel, R.; Okur, A.; Strockbine, B.; Roitberg, A.; Simmerling, C. Comparison of Multiple Amber Force Fields and Development of Improved Protein Backbone Parameters. *Proteins: Struct., Funct., Bioinf.* **2006**, *65*, 712−725.
(42) Bohr, H. G.; Jalkanen, K. J.; Elstner, M.; Frimand, K.; Suhai, S. A Comparative Study of MP2, B3LYP, RHF and SCC-DFTB Force Fields in Predicting the Vibrational Spectra of N-Acetyl-L-Alanine-N ′-Methyl Amide: VA and VCD Spectra. *Chem. Phys.* **1999**, *246*, 13−36.
(43) Han, W.-G.; Jalkanen, K. J.; Elstner, M.; Suhai, S. Theoretical Study of Aqueous N -Acetyl- L -Alanine N ′-Methylamide: Structures and Raman, VCD, and ROA Spectra. *J. Phys. Chem. B* **1998**, *102*, 2587−2602.
(44) Elstner, M.; Frauenheim, T.; Kaxiras, E.; Seifert, G.; Suhai, S. A Self-Consistent Charge Density-Functional Based Tight-Binding Scheme for Large Biomolecules. *Phys. Status Solidi* **2000**, *217*, 357−376.
(45) Elstner, M.; Hobza, P.; Frauenheim, T.; Suhai, S.; Kaxiras, E. Hydrogen Bonding and Stacking Interactions of Nucleic Acid Base Pairs: A Density-Functional-Theory Based Treatment. *J. Chem. Phys.* **2001**, *114*, 5149.
(46) Elstner, M. The SCC-DFTB Method and Its Application to Biological Systems. *Theor. Chem. Acc.* **2005**, *116*, 316−325.
(47) Elstner, M.; Cui, Q.; Munih, P.; Kaxiras, E.; Frauenheim, T.; Karplus, M. Modeling Zinc in Biomolecules with the Self Consistent Charge-Density Functional Tight Binding (SCC-DFTB) Method: Applications to Structural and Energetic Analysis. *J. Comput. Chem.* **2003**, *24*, 565−581.
(48) Xu, D.; Zhou, Y.; Xie, D.; Guo, H. Antibiotic Binding to Monozinc CphA Beta-Lactamase from Aeromonas Hydropila: Quantum Mechanical/molecular Mechanical and Density Functional Theory Studies. *J. Med. Chem.* **2005**, *48*, 6679−6689.
(49) Xu, D.; Xie, D.; Guo, H. Catalytic Mechanism of Class B2Metallo-Beta-Lactamase. *J. Biol. Chem.* **2006**, *281*, 8740−8747.
(50) Xu, D.; Guo, H.; Cui, Q. Antibiotic Binding to Dizinc Beta-Lactamase L1 from Stenotrophomonas Maltophilia: SCC-DFTB/CHARMM and DFT Studies. *J. Phys. Chem. A* **2007**, *111*, 5630−5636.
(51) Wu, S.; Xu, D.; Guo, H. QM/MM Studies of Monozinc B-Lactamase CphA Suggest That the Crystal Structure of an Enzyme-Intermediate Complex Represents a Minor Pathway. *J. Am. Chem. Soc.* **2010**, *132*, 17986−17988.
(52) Zheng, M.; Xu, D. New Delhi Metallo-B-Lactamase I: Substrate Binding and Catalytic Mechanism. *J. Phys. Chem. B* **2013**, *117*, 11596−11607.
(53) Xu, Q.; Guo, H.; Wlodawer, A.; Guo, H. The Importance of Dynamics in Substrate-Assisted Catalysis and Specificity. *J. Am. Chem. Soc.* **2006**, *128*, 5994−5995.
(54) Xu, D.; Guo, H. Quantum Mechanical/molecular Mechanical and Density Functional Theory Studies of a Prototypical Zinc Peptidase (carboxypeptidase A) Suggest a General Acid-General Base Mechanism. *J. Am. Chem. Soc.* **2009**, *131*, 9780−9788.
(55) Wu, S.; Zhang, C.; Cao, R.; Xu, D.; Guo, H. pH-Dependent Reactivity for Glycyl-L-Tyrosine in Carboxypeptidase-A-Catalyzed Hydrolysis. *J. Phys. Chem. B* **2011**, *115*, 10360−10367.
(56) Zhang, C.; Wu, S.; Xu, D. Catalytic Mechanism of Angiotensin-Converting Enzyme and Effects of the Chloride Ion. *J. Phys. Chem. B* **2013**, *117*, 6635−6645.
(57) Hou, G.; Cui, Q. Stabilization of Different Types of Transition States in a Single Enzyme Active Site: QM/MM Analysis of Enzymes in the Alkaline Phosphatase Superfamily. *J. Am. Chem. Soc.* **2013**, *135*, 10457−10469.
(58) Riccardi, D.; Yang, S.; Cui, Q. Proton Transfer Function of Carbonic Anhydrase: Insights from QM/MM Simulations. *Biochim. Biophys. Acta* **2010**, *1804*, 342−351.
(59) Han, W.-G.; Elstner, M.; Jalkanen, K. J.; Frauenheim, T.; Suhai, S. Hybrid SCC-DFTB/Molecular Mechanical Studies of H-Bonded Systems and of N-Acetyl-(L-Ala)n N′-Methylamide Helices in Water Solution. *Int. J. Quantum Chem.* **2000**, *78*, 459−479.
(60) Seabra, G.; Walker, R. C.; Elstner, M.; Case, D. A.; Roitberg, A. E.; Seabra, G. M. Implementation of the SCC-DFTB Method for Hybrid QM/MM Simulations within the Amber Molecular Dynamics Package. *J. Phys. Chem. A* **2007**, *111*, 5655−5664.
(61) Case, D. A.; Darden, T. A.; T.E. Cheatham, I.; Simmerling, C. L.; Wang, J.; Duke, R. E.; Luo, R.; Walker, R. C.; Zhang, W.; Merz, K. M.; Roberts, B.; Hayik, S.; Roitberg, A.; Seabra, G.; Swails, J.; Goetz, A. W.; Kolossváry, I.; Wong, K. F.; Paesani, F.; Vanicek, J.; Wolf, R. M.; P. A. Kollman AMBER 12, 2012.
(62) Xu, D.; Cui, Q.; Guo, H. Quantum Mechanical/molecular Mechanical Studies of Zinc Hydrolases. *Int. Rev. Phys. Chem.* **2014**, *33*, 1−41.
(63) Darden, T.; York, D.; Pedersen, L. Particle Mesh Ewald: An N·log(N) Method for Ewald Sums in Large Systems. *J. Chem. Phys.* **1993**, *98*, 10089.
(64) Adelman, S. A. Generalized Langevin Equation Approach for Atom/Solid-Surface Scattering: General Formulation for Classical Scattering off Harmonic Solids. *J. Chem. Phys.* **1976**, *64*, 2375.
(65) Berendsen, H. J. C.; Postma, J. P. M.; van Gunsteren, W. F.; DiNola, A.; Haak, J. R. Molecular Dynamics with Coupling to an External Bath. *J. Chem. Phys.* **1984**, *81*, 3684.
(66) Souaille, M.; Roux, B. Extension to the Weighted Histogram Analysis Method: Combining Umbrella Sampling with Free Energy Calculations. *Comput. Phys. Commun.* **2001**, *135*, 40−57.
(67) Amata, O.; Marino, T.; Russo, N.; Toscano, M. Human Insulin-Degrading Enzyme Working Mechanism. *J. Am. Chem. Soc.* **2009**, *131*, 14804−14811.
(68) Bora, R. P.; Ozbil, M.; Prabhakar, R. Elucidation of Insulin Degrading Enzyme Catalyzed Site Specific Hydrolytic Cleavage of Amyloid Beta Peptide: A Comparative Density Functional Theory Study. *J. Biol. Inorg. Chem.* **2010**, *15*, 485−495.
(69) Blumberger, J.; Lamoureux, G.; Klein, M. L. Peptide Hydrolysis in Thermolysin: Ab Initio QM/MM Investigation of the Glu143-Assisted Water Addition Mechanism. *J. Chem. Theory Comput.* **2007**, *3*, 1837−1850.
(70) Leissring, M. a; Lu, A.; Condron, M. M.; Teplow, D. B.; Stein, R. L.; Farris, W.; Selkoe, D. J. Kinetics of Amyloid Beta-Protein Degradation Determined by Novel Fluorescence- and Fluorescence Polarization-Based Assays. *J. Biol. Chem.* **2003**, *278*, 37314−37320.
(71) Simona, F.; Magistrato, A.; Dal Peraro, M.; Cavalli, A.; Vila, A. J.; Carloni, P. Common Mechanistic Features among Metallo-Beta-Lactamases: A Computational Study of Aeromonas Hydrophila CphA Enzyme. *J. Biol. Chem.* **2009**, *284*, 28164−28171.
(72) Simona, F.; Magistrato, A.; Vera, D. M. A.; Garau, G.; Vila, A. J.; Carloni, P. Protonation State and Substrate Binding to B2Metallo-

DOI: 10.1021/ci500544c
J. Chem. Inf. Model. 2015, 55, 72−83

Beta-Lactamase CphA from Aeromonas Hydrofila. *Proteins* **2007**, *69*, 595−605.
(73) Da Cruz, C. H. B.; Seabra, G. Molecular Dynamics Simulations Reveal a Novel Mechanism for ATP Inhibition of Insulin Degrading Enzyme. *J. Chem. Inf. Model.* **2014**, *54*, 1380−1390.
(74) Leissring, M. a; Lu, A.; Condron, M. M.; Teplow, D. B.; Stein, R. L.; Farris, W.; Selkoe, D. J. Kinetics of Amyloid Beta-Protein Degradation Determined by Novel Fluorescence- and Fluorescence Polarization-Based Assays. *J. Biol. Chem.* **2003**, *278*, 37314−37320.
(75) Bora, R. P.; Ozbil, M.; Prabhakar, R. Elucidation of Insulin Degrading Enzyme Catalyzed Site Specific Hydrolytic Cleavage of Amyloid Beta Peptide: A Comparative Density Functional Theory Study. *J. Biol. Inorg. Chem.* **2010**, *15*, 485−495.
(76) Bora, R. P.; Barman, A.; Zhu, X.; Ozbil, M.; Prabhakar, R. Which One among Aspartyl Protease, Metallopeptidase, and Artificial Metallopeptidase Is the Most Efficient Catalyst in Peptide Hydrolysis? *J. Phys. Chem. B* **2010**, *114*, 10860−10875.
(77) Wu, R.; Wang, S.; Zhou, N.; Cao, Z.; Zhang, Y. A Proton-Shuttle Reaction Mechanism for Histone Deacetylase 8 and the Catalytic Role of Metal Ions. *J. Am. Chem. Soc.* **2010**, *132*, 9471−9479.
(78) Malito, E.; Ralat, L.; Manolopoulou, M. Molecular Bases for the Recognition of Short Peptide Substrates and Cysteine-Directed Modifications of Human Insulin-Degrading Enzyme. *Biochemistry* **2008**, *47*, 12822−12834.
(79) Song, E.-S.; Juliano, M. A.; Juliano, L.; Hersh, L. B. Substrate Activation of Insulin-Degrading Enzyme (insulysin). A Potential Target for Drug Development. *J. Biol. Chem.* **2003**, *278*, 49789−49794.
(80) Kukday, S. S.; Manandhar, S. P.; Ludley, M. C.; Burriss, M. E.; Alper, B. J.; Schmidt, W. K. Cell-Permeable, Small-Molecule Activators of the Insulin-Degrading Enzyme. *J. Biomol. Screen.* **2012**, *17*, 1348−1361.
(81) Çakir, B.; Dağliyan, O.; Dağyildiz, E.; Bariş, İ.; Kavakli, I. H.; Kizilel, S.; Türkay, M. Structure Based Discovery of Small Molecules to Regulate the Activity of Human Insulin Degrading Enzyme. *PLoS One* **2012**, *7*, e31787.
(82) Im, H.; Manolopoulou, M.; Malito, E.; Shen, Y.; Zhao, J.; Neant-Fery, M.; Sun, C.-Y.; Meredith, S. C.; Sisodia, S. S.; Leissring, M. A.; Tang, W.-J. Structure of Substrate-Free Human Insulin-Degrading Enzyme (IDE) and Biophysical Analysis of ATP-Induced Conformational Switch of IDE. *J. Biol. Chem.* **2007**, *282*, 25453−25463.
(83) Grasso, G.; Rizzarelli, E.; Spoto, G. Human Insulin-Degrading Enzyme Working Mechanism. *J. Mass Spectrom.* **2009**, *44*, 735−741.
(84) Jeffrey, G. A. *An Introduction to Hydrogen Bonding*; Topics in Physical Chemistry; Oxford University Press: Oxford, U.K., 1997; p 303.

DOI: 10.1021/ci500544c
J. Chem. Inf. Model. 2015, 55, 72−83